

# Looking forward to forward physics at the CERN's LHC

Luis A. Anchordoqui

<sup>1</sup>Department of Physics and Astronomy, Lehman College, City University of New York, NY 10468, USA

**Abstract.** For decades, new physics searches in collider experiments have focused on the high- $p_T$  region. However, it has recently become evident that the LHC physics potential has not been fully exploited. To be specific, forward collisions, which produce particles along the beamline with enormous rates, have been almost completely ignored. For all practical purposes, these collisions are a treasure trove of physics, containing the highest-energy neutrinos ever produced by humans, as well as possible evidence for dark matter, light and weakly-coupled particles, and new forces. In the upcoming LHC Run 3 the ForwArd Search ExpeRiment (FASER) and its cousin FASER $\nu$  will extend the LHC's physics potential. A continuation of this forward physics program for the HL-LHC aims at the Forward Physics Facility (FPF), with larger scale experiments. In this report, I give an overview of the physics motivations for FASER, FASER $\nu$ , and the FPF experiments, including both Standard Model and beyond Standard Model physics.

## 1 Introduction

For decades, new physics searches in particle colliders have focused on the high- $p_T$  region. This is appropriate for heavy, strongly interacting particles with small cross-sections,  $\mathcal{O}(\text{fb}) \lesssim \sigma_{\text{high-}p_T} \lesssim \mathcal{O}(\text{pb})$ . The Large Hadron Collider (LHC) after Run 3 will reach a total integrated luminosity of over  $300 \text{ fb}^{-1}$  and during its high-luminosity era (HL-LHC) will reach  $3 \text{ ab}^{-1}$ . Given these considerations, a total of  $10^3 \lesssim N_{\text{events}}^{\text{high-}p_T} \lesssim 10^6$  would be produced roughly isotropically at the HL-LHC. In the last few years it has become evident that the LHC physics potential has not been fully exploited. Sure enough, low- $p_T$  forward collisions, with a total cross-section  $\sigma_{\text{low-}p_T} \sim \mathcal{O}(100 \text{ mb})$ , have been almost completely ignored. For HL-LHC, this cross-section corresponds to  $N_{\text{events}}^{\text{low-}p_T} \sim 10^{17}$ . The Forward Physics Facility (FPF) is one of the proposals to design and install dedicated far-forward physics experiments at the HL-LHC [1, 2]. In this report, I give an overview of the physics motivations for the FPF experiments, including both Standard Model (SM) and beyond Standard Model (BSM) physics.

## 2 BSM Physics Landscape

The ATLAS and CMS detectors are designed to find new heavy particles which are produced at rest and decay isotropically. However, as more and more high-energy data are being collected and analyzed at the LHC, the high-mass reach becomes saturated. Our best chance to discover BSM physics is to look in places that have not been explored before. As can be seen in Fig. 1, this means low masses and weak couplings. Now, these new light particles are mainly produced along the beam line and so they

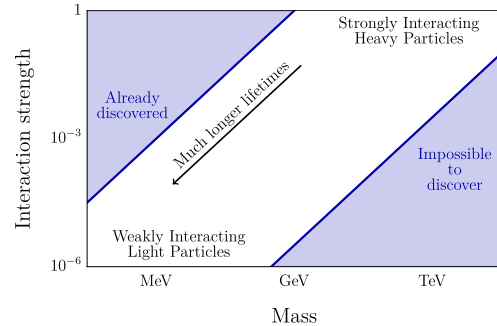


Figure 1. The new particle landscape. Adapted from [3].

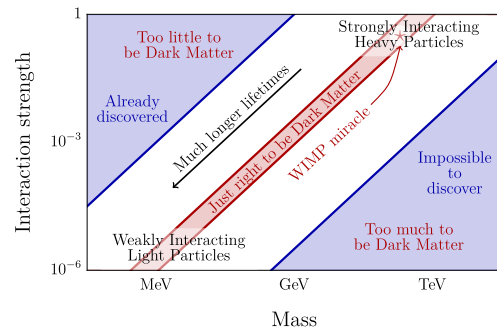


Figure 2. The thermal relic landscape. Adapted from [3].

would disappear through the holes that let the beams in. We need a detector to cover the blind spots in the forward region. High masses and weak couplings are also compelling, but are unlikely to be accessible in the near future.

We have pencilled out the purely particle physics approach to new physics searches. We can also adopt the

cosmological perspective for new physics searches. To carry out this task we assume there is a hidden sector with some dark matter (DM) in it. We further assume that the DM interacts with the SM sector through a portal, which can be characterized by a dark photon of mass  $m_{A'}$  and coupling  $\epsilon$ . If this were the case, then we could calculate the interaction annihilation cross-section, which parametrically goes as  $\epsilon^2$  and by dimensional analysis scales as  $m_{A'}^{-2}$ , yielding

$$\langle\sigma v\rangle\sim\epsilon^2/m_{A'}^2. \quad (1)$$

Finally, armed with (1) we would estimate where in the (mass, interaction strength) plane we have the right amount of DM to accommodate the thermal relic density. This is shown in Fig. 2 as a red band. We know that this band coincides with the frontier of High Energy Physics experiments, because it spans the parameter space of the well-known *WIMP miracle* [4]. The parametrization given in (1) predicts that new particles with low masses and weak couplings inside the red band can also accommodate the thermal relic density. It is just an incredible coincidence that the cosmological motivation and the particle physics motivation line up so beautifully in the (mass, interaction strength) plane.

The dark photons may decay to visible particles but only after traveling a long distance. The particle's velocity is near the speed of light  $v\sim 1$ , its rest lifetime is enhanced by the low mass and the small coupling  $\tau\propto\epsilon^{-2}m_{A'}^{-1}$ , and the lifetime is further enhanced by time dilation  $\gamma\propto E/m_{A'}$ , hence the distance travelled is

$$L=\gamma v\tau\sim 100\,m\left(\frac{10^{-5}}{\epsilon}\right)^2\left(\frac{100\,\text{MeV}}{m_{A'}}\right)^2\left(\frac{E}{\text{TeV}}\right). \quad (2)$$

Altogether, weakly coupled particles imply long lifetimes, whereas low masses typically makes particle production to peak in the forward direction. Optimally, what we need is a precision spectrometer looking into the forward region of LHC collisions. But of course, we cannot place a reasonable size detector on the beamline near the interaction point (IP), because it would block the proton beams. However, since the particles we are looking for are long-lived and weakly-interacting we can place a detector far upstream along the “line of sight” after the beams curve. This is the idea behind the ForWArD Search Experiment (FASER), which has been installed 480 m downstream of the ATLAS IP in the unused service tunnel and it is ready to start taking data during Run 3 [5].<sup>1</sup> It is also of interest to ask ourselves how big the detector has to be. For a pseudorapidity  $\eta\sim 9$ , the opening angle is  $\theta\simeq 2e^{-\eta}\sim 0.25$  mrad. Therefore, most of the long-lived particle (LLP) signal would go through one sheet of paper at 480 m.

To appreciate the physics potential of FASER2 next we examine in detail a specific model. The minimal dark photon portal with renormalizable couplings is generated by a hidden broken  $U(1)'$  gauge symmetry whose field strength tensor,  $F'_{\mu\nu}$ , kinetically mixes with the SM hypercharge

field strength tensor,  $B_{\mu\nu}$ , through the operator  $F'_{\mu\nu}B^{\mu\nu}$  [7]. After electroweak symmetry breaking, and with the gauge boson kinetic terms diagonalized, the dark photon develops a suppressed coupling to the electromagnetic (EM) current,  $J_{\text{EM}}^\mu$ . The renormalizable Lagrangian density of the model can be expressed in terms of the visible (SM) and dark sectors

$$\mathcal{L}=\mathcal{L}_{\text{SM}}+\mathcal{L}_{\text{dark}}, \quad (3)$$

with

$$\mathcal{L}_{\text{dark}}\supset -\frac{1}{4}F'_{\mu\nu}F'^{\mu\nu}+\frac{1}{2}m_{A'}^2A'^\mu A'_\mu+\epsilon e A'_\mu J_{\text{EM}}^\mu, \quad (4)$$

where the form of the  $A'$ -DM interaction  $\mathcal{L}_{A'\chi\bar{\chi}}$  is left unspecified, and where  $\chi$  denotes the DM particle. This model is characterized by three a priori unknown parameters:  $m_{A'}$ ,  $\epsilon$ , and the decay branching fraction  $\mathcal{B}(A'\rightarrow\chi\bar{\chi})$ . Throughout we assume that the dark matter particles are heavy such that the invisible dark-sector final states are not kinematically allowed because  $m_{A'}<2m_\chi$ . Given these considerations, the phase space to be probed by FASER2 can be described in the familiar  $(m_{A'},\epsilon)$  plane introduced in Figs. 1 and 2.

At hadron colliders like the LHC, dark photons can be abundantly produced through proton bremsstrahlung or via the decay of heavy mesons. For example, the expected branching fraction of  $\pi^0$  decay is found to be

$$\mathcal{B}(\pi^0\rightarrow\gamma A')=2\epsilon^2\left(1-\frac{m_{A'}^2}{m_{\pi^0}^2}\right)^3\mathcal{B}(\pi^0\rightarrow\gamma\gamma); \quad (5)$$

similar expressions can be obtained for  $\eta$ ,  $B$ , and  $D$  mesons. Indeed, over the lifetime of the HL-LHC there will be  $4\times 10^{17}$  neutral pions,  $6\times 10^{16}$   $\eta$  mesons,  $2\times 10^{15}$   $D$  mesons, and  $10^{13}$   $B$  mesons produced in the direction of FASER2. The partial decay width of  $A'$  to SM leptons is given by

$$\Gamma_{A'\rightarrow\ell^+\ell^-}=\frac{\epsilon^2\alpha_{\text{EM}}}{3}m_{A'}\left(1+2\frac{m_\ell^2}{m_{A'}^2}\right)\sqrt{1-4\frac{m_\ell^2}{m_{A'}^2}}, \quad (6)$$

where  $\alpha_{\text{EM}}$  is the fine structure constant,  $\ell=e,\mu,\tau$ , and  $m_{A'}>2m_\ell$  [8]. The partial decay width of  $A'$  to SM hadrons can be extracted from the measured value of  $\mathcal{R}_\mu\equiv\sigma_{e^+e^-\rightarrow\text{hadrons}}/\sigma_{e^+e^-\rightarrow\mu^+\mu^-}$  at center-of-mass energy equal to  $m_{A'}$ , and is given by

$$\Gamma_{A'\rightarrow\text{hadrons}}=\Gamma_{A'\rightarrow\mu^+\mu^-}\times\mathcal{R}_\mu(m_{A'}). \quad (7)$$

Loop-induced SM decays ( $A'\rightarrow 3\gamma$  and  $A'\rightarrow\nu\bar{\nu}$ ) are highly suppressed. In Fig. 3 we show the  $U(1)'$  sensitivity reach contour of FASER2 in the  $(m_{A'},\epsilon)$  plane, as obtained with the FORSEE package [9].

So far we have left the strength of the kinetic mixing completely unknown and model independent. We now consider a specific Little String Theory (LST) model, in which the weakness of gravity (or equivalently the enormity of the Planck mass) is attributed to the tiny value of the string coupling  $g_s$  [10]. In spite of the small  $g_s$ , in type II string theories with gauge interactions localized in the

<sup>1</sup>The acronym recalls another instrument that harnessed highly collimated particles and that was used to explore strange new worlds [6].

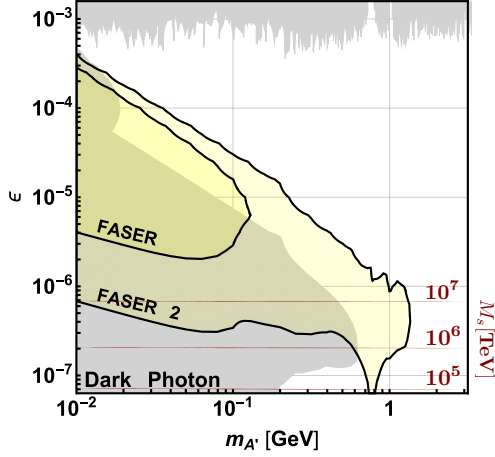


**Figure 3.** Dark photon sensitivity reach contour in the  $(m_{A'}, \epsilon)$  plane obtained with the FORSEE package [9]. The grey shaded regions are excluded by previous experiments. The vertical axis on the right indicates the  $\epsilon \Leftrightarrow M_s$  connection in LST models [11]. Adapted from [16].

vicinity of Neveu-Schwarz (NS) 5-branes, the SM gauge couplings are of order one and are associated with the sizes of compact dimensions.

The internal space is taken to be a product of a two-dimensional space, of volume  $V_2$ , times a four-dimensional compact space, of volume  $V_4$ . The relation between the Planck mass  $M_{\text{Pl}}$  and the string scale  $M_s$  is given by

$$M_{\text{Pl}}^2 = \frac{8}{g_s^2} M_s^8 \frac{V_2 V_4}{(2\pi)^6}, \quad (8)$$

with all the internal space radii of the order of the string length, i.e.,  $M_s^6 V_2 V_4 \simeq (2\pi)^6$ . The hierarchy problem is equivalent to understanding the smallness of  $g_s$ . The  $U(1)'$  lives on a D7-brane that wraps a 4-cycle of volume  $V_4$  and its remaining four dimensions extend into the uncompactified space-time. We remind the reader that within LST models the SM lives on NS5 branes, but since the  $U(1)'$  gauge boson comes from D-branes the SM is generically neutral under  $U(1)'$  as desired. The  $U(1)'$  gauge coupling is found to be [11]:

$$g' \simeq 32^{1/4} \sqrt{\pi} \sqrt{M_s/M_{\text{Pl}}}. \quad (9)$$

The mass of the dark photon is usually generated through spontaneous symmetry breaking; namely, through the vacuum expectation value (vev) of a hidden SM singlet Higgs field which carries a  $U(1)'$  charge. In LST models this is possible provided we tolerate a hierarchy between the vev and  $M_s$  that increases as  $M_s^{3/2}$  [11]. As noted above, the  $U(1)'$  does not couple directly to the visible sector, but does it via kinetic mixing with the hypercharge. This coupling is generated by loops of heavy dark states carrying charges  $(q^{(i)}, q'^{(i)})$  under the two  $U(1)$ 's and having masses  $M_i$ ,

$$\epsilon = \frac{eg'}{16\pi^2} \sum_i q^{(i)} q'^{(i)} \ln \frac{M_i^2}{\mu^2} \equiv \frac{eg'}{16\pi^2} C_{\text{Log}}, \quad (10)$$

where  $\mu^2$  denotes the renormalization scale (which in string theory is replaced by  $M_s$ ),  $e$  is the elementary

charge, and where we absorbed also the constant contribution in  $C_{\text{Log}} \sim 3$  [11]. Substituting (9) into (10) we obtain the region of the parameter space to be probed by FASER2, which is shown in Fig. 3.

The dark sector may include more than one mediator particle coupled to the visible sector. SM gauge and Lorentz symmetries greatly restrict the ways in which mediators can couple to SM interactions. Portals relevant for dark sector SM interactions depend on mediator spin and parity. FASER2 will not only be sensitive to the spin-1 vector gauge boson, but also to the spin-0 dark Higgs boson [12], the spin- $\frac{1}{2}$  sterile neutrino [13], and pseudo-scalar axions [14]. What's more, DM particles could scatter inside FPF dedicated neutrino experiments like FASERv2, the Advanced Scattering and Neutrino Detector (AdvSND), and the Forward Liquid Argon Experiment (FLArE) producing visible signals [15].<sup>2</sup> For example, elastic scattering of DM particles may be visible as an excess of neutrino-like events over the SM yield, whereas inelastic DM scattering could appear as an excess of the ratio of neutral-to-charged current-like events,  $r = N_{\text{NC}}/N_{\text{CC}}$ , over the SM prediction  $r \approx 0.31$ . SND@LHC allows measuring  $r$  with an accuracy  $(\Delta r/r)_{\text{SND@LHC}} = 10\%$  and the advanced configurations will reach  $(\Delta r/r)_{\text{AdvSND}} = 1\%$ . On top of the rich experimental program to search for scattering of DM particles the FORward MicroCharge SeArch (FORMOSA) detector is primarily targeted at probing the kinetic mixing portal [17], which allows DM from a hidden sector to become visible by acquiring a small electric charge, often called *millicharge* [18]. FORMOSA will reach sensitivity to charges as low as  $10^{-4}e$ . This will allow FORMOSA to provide the best probe of millicharged particles with mass between  $0.1 < m/\text{GeV} < 100$ . For a thorough discussion of BSM physics searches at the FPF and a complete list of references, see [1, 2].

In closing, we note that other proposed experiments at CERN which could provide complementary measurements of new LLPs include SHiP [19], FACET [20], and MATHUSLA [21].

### 3 Astroparticle Physics

Experiments at the FPF will also lay out opportunities for interdisciplinary studies at the intersection of high-energy particle physics and astroparticle physics. This is feasible by looking at the large flux of LHC neutrinos, which can be probed in low-background environments at a safe distance away from the interaction point and accelerator infrastructure. LHC neutrinos originate in the decay of charged pions, kaons, hyperons and charmed hadrons, making the measurement of the neutrino flux a unique probe of forward particle production. The feasibility of such LHC neutrino measurements has recently been demonstrated with the FASER prototype, which observed the first neutrino interaction candidates at the LHC [22].

<sup>2</sup>The Advanced SND project is meant to extend the physics case of the SND@LHC experiment. It will consist of two detectors: one placed in the same  $\eta$  region as SND@LHC, i.e.  $7.2 < \eta < 8.4$ , dubbed FAR, and the other one in the region  $4 < \eta < 5$ , dubbed NEAR. The FPF would host the FAR detector.

### 3.1 Forward strangeness production

Ultra-high-energy cosmic rays (UHECRs) supply a particle beam without financial burden to study collisions at center-of-mass (c.m.) energies and kinematic regimes not accessible at terrestrial colliders [23]. For example, the scattering in air of a cosmic  ${}^4\text{He}$  nucleus with energy  $E = 10^{10.3}$  GeV reaches a c.m. energy in the nucleon-nucleon system of  $\sqrt{s_{NN}} \sim \sqrt{2E_N m_N} \sim 100$  TeV, where  $E_N \simeq 10^{9.7}$  GeV is the cosmic ray energy per nucleon in the fixed target frame and  $m_N$  is the iso-scalar nucleon mass. The subsequent air shower is steered by hadron-nucleus collisions with low momentum transfer in the non-perturbative regime of QCD. The shower description is therefore based on phenomenological models, which are inspired by  $1/N$  QCD expansion and are also supplemented with generally accepted theoretical principles like duality, unitarity, Regge behavior, and parton structure. But of course, these phenomenological models are inherently uncertain due to: (i) the lack of a fundamental theoretical description of soft hadronic and nuclear interactions; (ii) the large extrapolation required from collider energies to the UHECR range. For example, a major source of uncertainty in modeling UHECR interactions is encrypted in the extrapolation of the measured parton densities several orders of magnitude down to low Bjorken- $x$ . UHECRs that impact on the upper atmosphere with  $E_N \sim 10^{9.7}$  GeV yield partons with  $x \sim m_\pi / \sqrt{s_{NN}} \sim 10^{-6}$ , *viz.* far smaller than anything accessible at today's accelerators.

Along this line, data from the Pierre Auger Observatory suggest that the hadronic component of showers (initiated by cosmic rays with energy  $10^{9.8} < E/\text{GeV} < 10^{10.2}$ ) contains about 30% to 60% more muons than expected from simulations based on hadronic interaction models tuned to accommodate LHC data [24]. The significance of the discrepancy between data and model prediction is somewhat above  $2.1\sigma$ . The discrepancy between experiment and simulations has also been observed in the Telescope Array data analysis [25].<sup>3</sup>

To date the best hope for resolving the muon mismatch involves decreasing the energy fraction lost to photon production (dominantly from  $\pi^0$  decay) in the description of hadronic collisions, because this is the only known modification of the cascade development which increases the mean muon number without encountering any restrictions from other shower observables [27]. The required suppression of pion production could come from an enhancement of strangeness production [28].<sup>4</sup> Indeed, one could expect heavy flavor production to be enhanced in kinematic regimes where quark masses may be insignificant.

The amount of forward strangeness production is traced by the ratio of charged kaons to pions, for which the ratio of electron and muon neutrino fluxes is a proxy that will be measured by FASERv2 and FLArE. Note that

pions primarily decay into muon neutrinos, whereas kaon decays lead to fluxes of both electron and muon neutrinos. On top of that, muon and electron neutrinos with different parent mesons populate different energy regions, and so the spectral shape can be used to disentangle the neutrino origin. Moreover, given that  $m_\pi < m_K$ , neutrinos from pion decay are more concentrated around the line-of-sight than those of kaon origin, and hence neutrinos from pions obtain less additional transverse momentum than those from kaon decays. Accordingly, the closeness of the neutrinos to the line-of-sight, or equivalently their rapidity distribution, can also be used to disentangle different neutrino origins and estimate the pion to kaon ratio.

To estimate the sensitive of FPF experiments for measuring forward strangeness production we thus investigate the sensitivity to the associated dominant channel, which is discernible from the pion-to-kaon ratio. In Fig. 4, we show the expected number of neutrino interactions with the FASERv detector, assuming a  $25 \text{ cm} \times 25 \text{ cm}$  cross sectional area and a 1.2 ton target mass, as a function of the neutrino energy. Here, we have used Sibyll-2.3d [30] as primary generator and use the fast LHC neutrino flux simulation introduced in [31] to describe the propagation and decay the long-lived hadrons in the LHC beam pipe.<sup>5</sup> The origin of the neutrinos is indicated by the different line colors: red for pion decay, blue for kaon decay, magenta for hyperon decay, and green for charm decay. As explained above, the neutrinos from pions and kaons populate different regions of phase space, which can be used to disentangle pion and kaon production. In Fig. 5, we show the results for the FLArE detector at the FPF, which is assumed to have a  $1 \text{ m} \times 1 \text{ m}$  cross sectional area and a 10 ton target mass.

In Fig. 4 and Fig. 5, we also show how a  $\pi \leftrightarrow K$  swapping with probability given by

$$F_s(\eta) = \begin{cases} f_s & \text{if } -\infty < \eta < -\eta_0 \\ 0 & \text{if } -\eta_0 \leq \eta \leq \eta_0 \\ f_s & \text{if } \eta_0 < \eta < \infty \end{cases}, \quad (11)$$

changes the expected neutrino fluxes and event rates for the considered experiments, where  $\eta$  is the pseudorapidity in the center-of-mass frame,  $\eta_0 = 4, 6, 8$  and  $0 < f_s < 1$ . For  $f_s > 0$ , the particle species are changed according to the following criteria: (i) each  $\pi^0$  is transformed onto  $K_S^0$  or  $K_L^0$ , with 50% chance between them; (ii) each  $\pi^+$  ( $\pi^-$ ) is transformed onto  $K^+$  ( $K^-$ ) [33]. As expected, positive values of  $f_s$  lead to a suppression of the neutrino flux from pions as well as a larger relative enhancement of the neutrino flux from kaons. This is due to the initially roughly 10 times larger flux of pions, such that even a small rate of  $\pi \leftrightarrow K$  swapping can substantially increase the neutrino flux from the kaon decays. This leads to the remarkable result that already for  $f_s = 0.1$  ( $f_s = 0.2$ ) the predicted electron neutrino flux at the peak of the spectrum is a factor of 1.6 (2.2) larger. These differences are significantly larger than the anticipated statistical uncertainties at the FPF [1, 31]. We can see that there is almost

<sup>3</sup>We note that the muon deficit of simulated events is not observed in IceTop data with  $10^{6.4} < E/\text{GeV} < 10^{8.1}$  [26]. However, the c.m. energy per nucleon pair of these showers is well below those of LHC collisions.

<sup>4</sup>A point worth noting at this juncture is that the strange fireball model put forward in [28] could only be the carrier of subdominant effects [29].

<sup>5</sup>The hadronic interaction model Sibyll-2.3d yields the smallest muon mismatch between data and simulations [32].

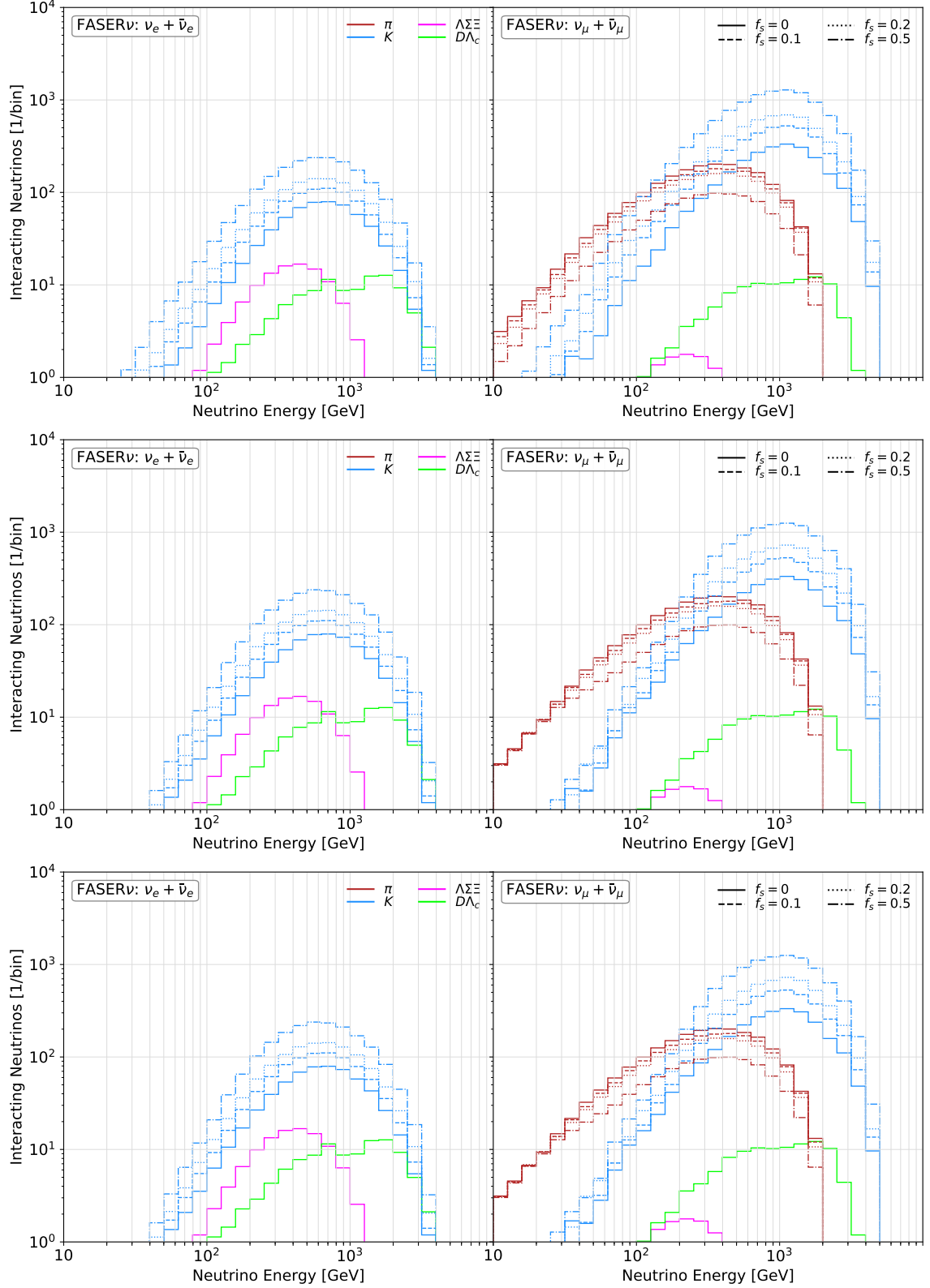


**Figure 4.** Energy spectrum of electron neutrinos (left) and muon neutrinos (right) interacting with FASERν. The vertical axis shows the number of charged current neutrino interactions per energy bin for an integrated luminosity of  $150 \text{ fb}^{-1}$  by different colors: pion decays (red), kaon decays (blue), hyperon decays (magenta), and charm decays (green). The different line styles correspond to predictions obtained from Sibyll-2.3d with secondary pions processed using  $F_s(\eta)$ , for different values of  $f_s$ . We have taken  $\eta_0 = 4, 6, 8$  from top to bottom. The image on the 1st row is taken from [33], while the images on the 2nd and 3rd rows are courtesy of Felix Kling.

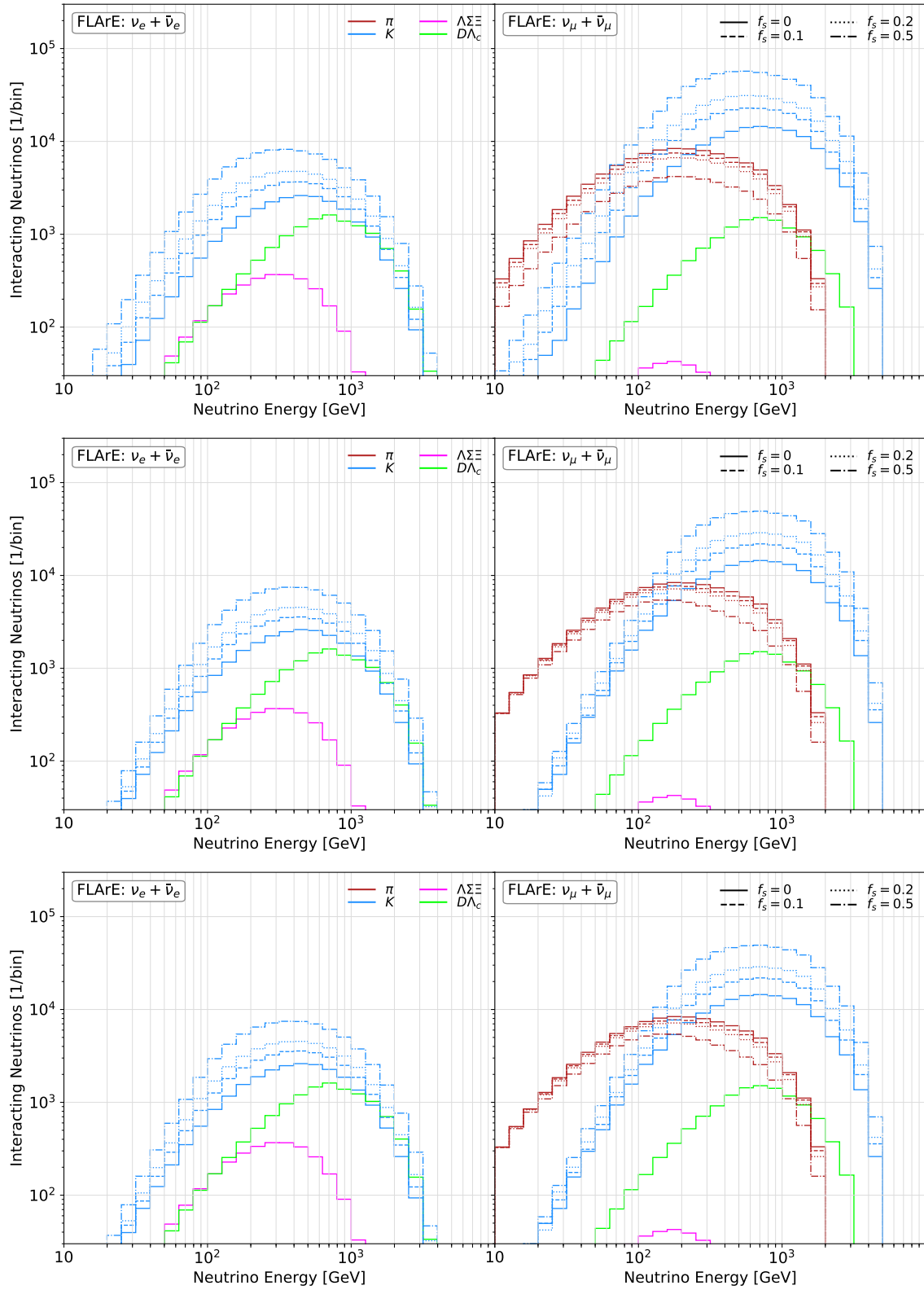


**Figure 5.** Expected number of charged current neutrino interactions with the FLArE detector at the FPF assuming an integrated luminosity of  $3 \text{ ab}^{-1}$ . See Fig. 4 for details.

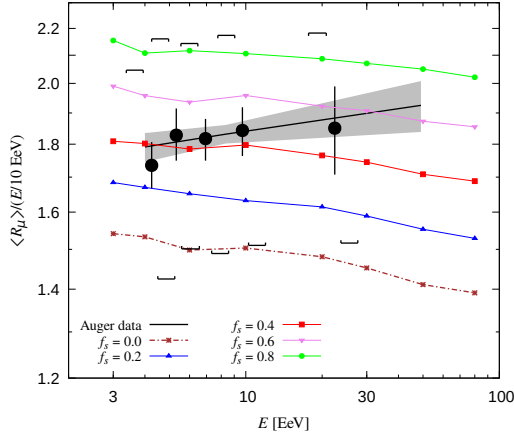


**Figure 6.** The dimensionless muon content  $\langle R_\mu \rangle = N_\mu / N_{\mu,10}$ , where  $N_\mu$  is the total number of muons at ground level and  $N_{\mu,10}$  is the average number of muons in simulated showers of protons with  $E = 10^{10}$  GeV and incident angle of  $67^\circ$ .  $\langle R_\mu \rangle$  results from air shower simulations for different values of  $f_s$  and  $\eta_0 = 4$  are superimposed over Auger data with statistical ( $\blacklozenge$ ) and systematic ( $\square$ ) uncertainties [34]. The simulations have been carried out with AIRES [35] + Sibyll-2.3d assuming a nuclear composition of UHECRs derived from partial fluxes of the fit reported by the Pierre Auger Collaboration [36]. For details, see [33].

no variation in the neutrino flux while changing  $\eta_0$  from 4 to 6. Requiring  $\eta_0 = 8$  mainly affects the lower energy part of the neutrino spectrum, and the effect of non-zero  $f_s$  becomes somewhat smaller. Altogether, we can conclude that FASER $\nu$  and FPF neutrino flux measurements will provide invaluable information to measure the rate of forward strangeness production through a measurement of the pion-to-kaon ratio. This measurement could become a unique asset in addressing the UHECR muon conundrum; see Fig. 6.

### 3.2 Forward charm production

Decays of mesons produced in air showers lead to a large flux of atmospheric neutrinos. The decay of charged pions determines the neutrino energy spectra up to about 100 GeV above which they become increasingly modified by the kaon contribution, which asymptotically reaches 90%. As can be seen in Fig. 7, above about  $10^{5.5}$  GeV, kaons are also significantly attenuated before decaying and the “prompt” component, arising mainly from very short-lived charmed hadrons ( $D^\pm$ ,  $D^0$ ,  $\bar{D}^0$ ,  $D_s^\pm$ ,  $B_c^\pm$ , and  $\Lambda_c$ ) dominates the spectrum. The flavor ratio of these prompt neutrinos is  $N_{\nu_e} : N_{\nu_\mu} : N_{\nu_\tau} \sim 12/25 : 12/25 : 1/25$ .

The neutrino flux arising from pion and kaon decay is reasonable well understood, with an uncertainty in the range 10% - 20% [37]. However, the understanding of the prompt neutrino flux is hampered by the large uncertainties in the QCD modeling of heavy meson production [41]. The cosmic neutrino flux is also subject to large uncertainties. A fit to IceCube cascade data assuming a single power

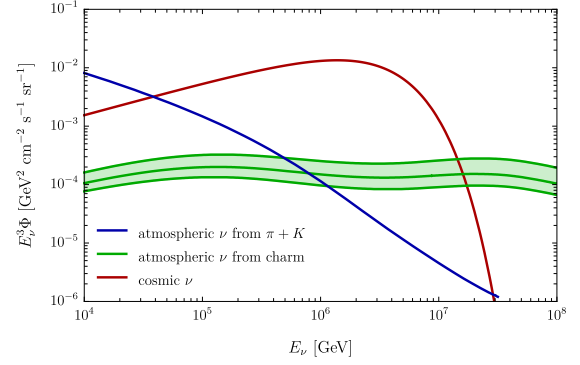


**Figure 7.** Atmospheric and cosmic neutrinos fluxes per neutrino flavor scaled by  $E_\nu^3$ . The blue curve shows the atmospheric neutrino flux produced via decay of pions and kaons [37]. The green band indicates the prompt atmospheric neutrino flux from perturbative charm production and its uncertainty [38]. The red curve denotes the flux of cosmic neutrinos from a fit to 6 yr of IceCube data [39]. IceCube’s 7.5 yr sample gives very similar results [40].

law spectrum with a cutoff yields,

$$\Phi = 3 \times 10^{-18} \Phi_0 \left( \frac{E_\nu}{E_0} \right)^{-\gamma} e^{-E_\nu/E_{\text{cut}}} (\text{GeV cm}^2 \text{s sr})^{-1}, \quad (12)$$

where  $E_\nu$  is the neutrino energy,  $\Phi_0 = 1.83^{+0.37}_{-0.31}$ ,  $\gamma = 2.45^{+0.09}_{-0.11}$ ,  $E_0 = 100$  TeV and  $\log_{10}(E_{\text{cut}}/\text{GeV}) = 6.4^{+0.9}_{-0.4}$  [39]. Note that the prompt neutrino flux could dominate the cosmic neutrino flux above  $10^{7.3}$  GeV. Besides, a major feature of the UHECR spectrum above  $10^{10}$  GeV is the increasing fraction of heavy nuclei with respect to light nuclei [42]. This implies that the cosmogenic neutrino flux could be strongly suppressed [43] and we may be witnessing the high-energy cutoff of cosmic neutrinos in IceCube data (without the need for Lorentz invariance violation [44]). All in all, it seems critical to obtain a robust measurement of the atmospheric charm production.

A determination of the prompt neutrino flux requires a calculation of the charm production differential cross-section  $d\sigma/dx_c$  followed by the hadronization of charm particles, where  $x_c$  is the longitudinal energy fraction of the produced charm quark [38]. Alternatively one uses the Feynman- $x$  variable

$$x_c \simeq x_F \equiv \frac{p_L^*}{|\max(p_L^*)|} \simeq \frac{2p_L^*}{\sqrt{s_{NN}}} = \frac{2m_T \sinh y^*}{\sqrt{s_{NN}}} \quad (13)$$

where  $m_T \sim 3$  GeV is the transverse mass, and  $p_L^*$  and  $y^*$  are the longitudinal momentum and rapidity in the center-of-mass frame. Now, Sibyll-2.3c predicts that for  $E_\nu \sim 10^7$  GeV, the probability density function of the parent nucleon energies peaks at  $E_N \sim 30 E_\nu$  [45]. If we approximate the energy of the charm meson as  $E_c \sim 3E_\nu$ , it follows that  $x_c \equiv E_c/E_N \sim 0.1$ . For large rapidity,  $\sinh y^* \simeq e^{y^*}/2$  and so (13) leads to

$$y^* \simeq \ln \left( \sqrt{6 m_N E_\nu x_c / m_T} \right). \quad (14)$$

Using (14) it is straightforward to verify that neutrinos with  $10^7 < E_\nu/\text{GeV} < 10^8$  span the forward rapidity range  $6.2 < y^* < 7.8$ .

All told, LHC neutrinos to be measured at the FPF experiments could give critical information on charm production at Feynman- $x$  close to 1. This process could potentially become a source of background for cosmic neutrinos with  $E_\nu \gtrsim 10^{7.3}$  GeV, and at the moment we have no data and we have no theory for the process.

## 4 Conclusions

The next breakthrough in particle physics is likely to involve LLPs. FPF experiments operating at the HL-LHC will be sensitive to an unexplored phase space for a broad range of LLP hidden sector physics. In addition, neutrino measurements at these experiments will improve the modeling of high-energy hadronic interactions in the atmosphere and consequently will reduce the associated uncertainties of air shower measurements.

## Acknowledgments

It is a pleasure to acknowledge many inspiring and fruitful discussions with Ignatios Antoniadis, Karim Benakli, Jonathan Feng, Carlos García Canal, Felix Kling, Dieter Lüst, Hallsie Reno, Sergio Sciutto, and Jorge Fernandez Soriano. This work has been supported by the U.S. NSF PHY-2112527 and NASA 80NSSC18K0464.

## References

- [1] L. A. Anchordoqui *et al.*, Phys. Rept. **968**, 1 (2022).
- [2] J. L. Feng *et al.*, arXiv:2203.05090.
- [3] J. L. Feng, talk at *Cosmic Controversies*, Kavli Institute for Cosmological Physics, Chicago (2019).
- [4] J. L. Feng, Ann. Rev. Astron. Astrophys. **48**, 495 (2010).
- [5] J. L. Feng, I. Galon, F. Kling and S. Trojanowski, Phys. Rev. D **97**, 035001 (2018).
- [6] J. L. Feng, talk at *New Probes for Physics Beyond the Standard Model*, KITP, Santa Barbara (2018).
- [7] B. Holdom, Phys. Lett. B **166**, 196 (1986).
- [8] P. Ilten, Y. Soreq, J. Thaler, M. Williams and W. Xue, Phys. Rev. Lett. **116**, 251803 (2016).
- [9] F. Kling and S. Trojanowski, Phys. Rev. D **104**, 035012 (2021).
- [10] I. Antoniadis, S. Dimopoulos and A. Givon, JHEP **05**, 055 (2001).
- [11] L. A. Anchordoqui, I. Antoniadis, K. Benakli and D. Lüst, arXiv:2204.06469.
- [12] B. Patt and F. Wilczek, arXiv:hep-ph/0605188.
- [13] M. Pospelov, A. Ritz and M. B. Voloshin, Phys. Lett. B **662**, 53-61 (2008).
- [14] Y. Nomura and J. Thaler, Phys. Rev. D **79**, 075008 (2009).
- [15] B. Batell, J. L. Feng and S. Trojanowski, Phys. Rev. D **103**, 075023 (2021).
- [16] A. Ariga *et al.*, arXiv:1901.04468.
- [17] H. Goldberg and L. J. Hall, Phys. Lett. B **174**, 151 (1986).
- [18] S. Foroughi-Abari, F. Kling and Y. D. Tsai, Phys. Rev. D **104**, 035014 (2021).
- [19] S. Alekhin *et al.*, Rept. Prog. Phys. **79**, 124201 (2016).
- [20] S. Cerci *et al.*, arXiv:2201.00019.
- [21] H. Lubatti *et al.*, JINST **15**, C06026 (2020).
- [22] H. Abreu *et al.*, Phys. Rev. D **104**, L091101 (2021).
- [23] L. A. Anchordoqui, Phys. Rept. **801**, 1 (2019).
- [24] A. Aab *et al.*, Phys. Rev. Lett. **117**, 192001 (2016).
- [25] R. Abbasi *et al.*, Phys. Rev. D **98**, 022002 (2018).
- [26] R. Abbasi *et al.*, arXiv:2201.12635.
- [27] J. Allen and G. Farrar, arXiv:1307.7131.
- [28] L. A. Anchordoqui, H. Goldberg and T. J. Weiler, Phys. Rev. D **95**, 063005 (2017).
- [29] L. A. Anchordoqui, C. García Canal, S. J. Sciutto and J. F. Soriano, Phys. Lett. B **810**, 135837 (2020).
- [30] F. Riehn, R. Engel, A. Fedynitch, T. K. Gaisser and T. Stanev, Phys. Rev. D **102**, 063002 (2020).
- [31] F. Kling and L. J. Nevay, Phys. Rev. D **104**, 113008 (2021).
- [32] S. J. Sciutto, EPJ Web Conf. **210**, 02007 (2019).
- [33] L. A. Anchordoqui, C. García Canal, F. Kling, S. J. Sciutto and J. F. Soriano, JHEAp **34**, 19 (2022).
- [34] A. Aab *et al.*, Phys. Rev. D **91**, 032003 (2015) [Phys. Rev. D **91**, 059901 (2015)].
- [35] S. J. Sciutto, arXiv:astro-ph/9911331; <http://aires.fisica.unlp.edu.ar>.
- [36] A. Aab *et al.*, JCAP **04**, 038 (2017) [JCAP **03**, E02 (2018)].
- [37] T. K. Gaisser and M. Honda, Ann. Rev. Nucl. Part. Sci. **52**, 153 (2002).
- [38] A. Bhattacharya, R. Enberg, M. H. Reno, I. Sarcevic and A. Stasto, JHEP **06**, 110 (2015).
- [39] M. G. Aartsen *et al.*, Phys. Rev. Lett. **125**, 121104 (2020).
- [40] R. Abbasi *et al.*, Phys. Rev. D **104**, 022002 (2021).
- [41] F. Halzen and L. Wille, Phys. Rev. D **94**, 014014 (2016).
- [42] A. A. Watson, JHEAp **33**, 14 (2022).
- [43] L. A. Anchordoqui, H. Goldberg, D. Hooper, S. Sarkar and A. M. Taylor, Phys. Rev. D **76**, 123008 (2007).
- [44] L. A. Anchordoqui, V. Barger, H. Goldberg, J. G. Learned, D. Marfatia, S. Pakvasa, T. C. Paul and T. J. Weiler, Phys. Lett. B **739**, 99 (2014).
- [45] A. Fedynitch, F. Riehn, R. Engel, T. K. Gaisser and T. Stanev, Phys. Rev. D **100**, 103018 (2019).